

1 **Estimating oceanic primary production using**
2 **vertical irradiance and chlorophyll profiles**
3 **from ocean gliders in the North Atlantic**

4
5 *Victoria S. Hemsley*^{1,2}, Timothy J. Smyth³, Adrian P. Martin², Eleanor Frajka-Williams¹,*
6 *Andrew F. Thompson⁴ Gillian Damerell⁵ and Stuart C. Painter²*

7
8 ¹ University of Southampton, National Oceanography Centre, European Way, Southampton,
9 SO14 3ZH, UK

10 ² National Oceanography Centre, Southampton, SO14 3ZH, UK

11 ³ Plymouth Marine Laboratory, Prospect Place, The Hoe, Plymouth, PL1 3DH, UK

12 ⁴ Environmental Science & Engineering, California Institute of Technology, Pasadena, US

13 ⁵ School of Environmental Sciences, University of East Anglia, Norwich, UK

14
15
16 Contact details

17 Victoria Hemsley

18 vsh1g12@soton.ac.uk

24 **Abstract**

25 An autonomous underwater vehicle (Seaglider) has been used to estimate marine primary
26 production (PP) using a combination of irradiance and fluorescence vertical profiles. This
27 method provides estimates for depth-resolved and temporally evolving PP on fine spatial
28 scales in the absence of ship-based calibrations. We describe techniques to correct for known
29 issues associated with long autonomous deployments such as sensor calibration drift and
30 fluorescence quenching. Comparisons were made between the Seaglider, stable isotope (^{13}C)
31 and satellite estimates of PP. The Seaglider-based PP estimates were comparable to both
32 satellite estimates and stable isotope measurements.

33

34 **Keywords:** AUV, glider, primary production, fluorescence profiles, North Atlantic.

35 **Introduction**

36 Primary production (PP) is the carbon fixed by plants through photosynthesis, the basis of
37 almost all terrestrial and marine food webs. Marine phytoplankton fix 45-50 Gt C yr⁻¹,
38 approximately half of global PP.^{1,2} PP is critical for regulating the drawdown of atmospheric
39 carbon dioxide³ and the air-sea exchange of radiatively important trace gases.⁴⁻⁶ In situ
40 measurements of PP in the open ocean are sparse and avoid winter, making it difficult to
41 resolve and separate spatial and temporal variability.¹ Regular fixed-point sampling is
42 difficult to extrapolate due to spatial variability. Satellites provide global estimates of oceanic
43 PP over a range of spatial and temporal scales⁷⁻¹¹ but, while satellite-derived surface
44 chlorophyll captures the variability in PP better than any other remotely sensed parameter,¹² it
45 relies on cloud free skies and only observes the top few metres, thereby omitting features
46 such as subsurface chlorophyll maxima (SCM).¹³ As a result, PP estimates derived
47 exclusively from satellite data typically underestimate spatial and temporal variability.¹
48 Methods have been developed to accommodate SCM,¹⁴ but are based on broad statistical
49 relationships.¹⁵

50

51 Significant improvements in PP estimates from satellite surface chlorophyll fields are
52 possible with simultaneous in situ chlorophyll and PAR profiles.¹² Underwater gliders
53 provide such data, improving the vertical and temporal resolution of observations.^{16,17}
54 However, gliders use fluorescence as proxy for chlorophyll¹⁹ and long-duration missions
55 may lack sufficient in situ calibration.^{18,20}

56

57 We describe a method for estimating PP at high vertical and temporal resolution, using glider
58 chlorophyll fluorescence and irradiance profiles. Significantly, it uses irradiance to calibrate

59 fluorescence, and therefore needs no in situ samples for calibration. This method makes
60 possible depth-resolved continuous estimates of PP over a full seasonal cycle, in all weather.

61

62

63 **2. Datasets**

64 **2.1 Area of Study**

65 Data were collected in the northeast Atlantic Ocean (48° 41' N, 16° 11' W) as part of the
66 OSMOSIS (Ocean Surface Mixing, Ocean Submesoscale Interaction Study). This site is
67 approximately 40 km southeast of the Porcupine Abyssal Plain sustained observatory (Figure
68 1).^{21,22}

69

70 Currents in this area are generally weak,^{23,24} with mean dive averaged currents of 11 cm s⁻¹.

71 Patchy phytoplankton distributions with fine spatial scales (<10 km) have been observed in
72 this region.²⁵ Diatoms dominate the spring bloom, succeeded by prymnesiophytes and

73 dinoflagellates.^{26, 27} In summer, diatoms form an SCM at the base of the mixed layer.^{28, 29}

74 Due to the patchy nature of the phytoplankton distribution, advection of spatial variability can
75 result in apparent variations in the phytoplankton community structure on daily timescales.³⁰

76

77 **2.2 Seaglider data**

78 A Seaglider is an autonomous, buoyancy driven vehicle that profiles to a depth of 1000 m
79 with a 0.5-1 m vertical sampling resolution along a saw-tooth trajectory.³¹⁻³³ Seaglider SG566
80 was deployed from April to September 2013 sampling a 15km x 15km area, following a
81 figure-of-eight path with an average 1000 m profiling time of 2.6 hours for an up/down cast
82 (Figure 1).

83

84 SG566 was equipped with an unpumped Seabird SBE13 CT sail (conductivity-temperature;
85 Seabird Electronics, Bellevue, USA), a Paine pressure sensor (Paine Electronics, East
86 Wenatchee, USA), a Triplet Ecopuck (Wetlabs, Philomath, USA) measuring chlorophyll
87 fluorescence and optical back scatter, and a broadband 4π cosine Photosynthetically Active
88 Radiation (PAR) sensor (400-700 nm; Biospherical Instruments, San Diego, USA). Raw
89 measurements from the CT sail were initially calibrated using manufacturer-supplied
90 coefficients, with further corrections to account for thermal lag.³⁴ Glider salinities were
91 calibrated against cruise data.³⁵ Pressure measurements were corrected to remove long term
92 drift and to account for pressure hysteresis within each dive.

93

94 Manufacturer calibrations were initially applied to data from the Wetlabs Triplet and 4π PAR
95 by subtracting the instrument blank and applying a scaling factor. The manufacturer's
96 calibration for chlorophyll fluorescence is based on the sensor's response to a culture of the
97 phytoplankton species *Thalassiosira weissflogii* at a known chlorophyll-*a* concentration
98 (Figure S3).³⁶ Our secondary calibration is outlined below. Other empirical methods have
99 been developed to calibrate fluorescence profiles including ones that take into account the
100 presence of an SCM²⁰ but by using in situ PAR data a scale factor can be derived which can
101 change dynamically and hence reflect changes in community composition (see Section 4.2).
102 The manufacturer's PAR sensor calibration uses a traceable 1000 watt type FEL Spectral
103 Irradiance Standard. All data were aggregated into 2 m depth intervals.

104

105 To obtain estimates of PP we used calibrated chlorophyll fluorescence, temperature and PAR
106 (Sections 2.5-2.7, Figure S1). Optical backscatter measurements were used to correct for
107 fluorescence quenching,³⁷ and temperature, salinity and density were used to estimate mixed
108 layer depths.

109

110 **2.3 In situ samples**

111 Three cruises to the survey region were conducted by the RRS *James Cook*: glider
112 deployment (JC085; April 14-29), mid-mission (JC087; June 1- 18) and glider recovery
113 (JC090; September 1-16). Water samples for chlorophyll-*a* were collected on all cruises
114 from up to six depths across the euphotic zone using a Seabird 911 plus CTD-Niskin rosette
115 system. Chlorophyll-*a* concentrations were measured using 250 ml water samples filtered
116 onto 25 mm Whatman glass fibre filters (GF/F; nominal pore size 0.7 μm). Chlorophyll-*a*
117 pigment was extracted in 6 ml of 90% acetone at 4°C in the dark for ~20 hours before
118 measurement on a Turner Designs Trilogy fluorometer calibrated against a pure chlorophyll
119 standard (spinach extract, Sigma Aldrich).³⁸ Two ship-fitted cosine collectors (Skye
120 Instruments, UK) measured incident PAR.

121

122 Measurements of PP using the ¹³C method³⁹ were made between 30th May and 18th June on
123 JC087 only. Water samples were collected from pre-dawn CTD casts at five depths: 55%,
124 20%, 7%, 5% and 1% of surface irradiance based on profiles obtained from previous midday
125 CTD casts. Each 1 litre water sample was added to an acid-rinsed Nalgene polycarbonate
126 bottle, which was wrapped with optical filters (Lee Filters, Hampshire, UK) to replicate the
127 appropriate irradiance levels. Each bottle was spiked with 200 μL of ¹³C labelled sodium
128 bicarbonate (0.65g in 50 ml of pH adjusted milli-Q water), corresponding to an addition of
129 255 $\mu\text{mol L}^{-1}$ (or ~1% of ambient (~2084 $\mu\text{mol L}^{-1}$) dissolved inorganic carbon
130 concentrations). Sealed sample bottles were placed in on-deck incubators, which were
131 flushed with surface seawater for 24 hours. Afterwards, each sample was filtered onto an
132 ashed (450°C, 6 hours) 25mm GF/F (Whatman) filter and rinsed with a weak HCl solution (1-
133 2%) to remove inorganic carbon before being stored frozen at -20°C. Filters were oven dried

134 and encapsulated in tin capsules. Samples were analysed for ^{13}C isotopic enrichment at the
135 Scottish Association for Marine Science using an ANCA NT preparation system coupled to a
136 PDZ 20-20 Stable Isotope Analyser (PDZ Europa Scientific Instruments, UK). PP was
137 calculated from the stable isotope results using standard equations.⁴⁰

138

139 **2.4 Satellite ocean colour data and primary production estimates**

140 We obtained 1 km resolution daily chlorophyll composites of MODIS Aqua data from the
141 NERC Earth Observation Data Acquisition and Analysis Service (NEODAAS). For each
142 Seaglider surfacing the satellite data pixel that matched the position and date was extracted.
143 Cloud cover resulted in data gaps in satellite coverage and surface match ups; these time
144 periods were omitted from the analysis.

145

146 Full depth profiles of chlorophyll were calculated for satellite data using statistical
147 relationships relating satellite chlorophyll to the shape of the chlorophyll profile at depth
148 (Supporting Information).¹⁴

149

150 For an alternative estimate of PP, for comparison to the glider-based estimates, these profiles
151 and surface PAR were inputs to a PP algorithm⁴¹ that couples the glider photosynthesis
152 model⁴² (Section 3.3) to the HYDROLIGHT radiative transfer code⁴³ which uses sea surface
153 temperature, PAR and day length to more accurately estimate irradiance with depth.

154

155 **2.5. Irradiance corrections, calibrations and calculation**

156 PP is best parameterised using spectral irradiance, as shorter wavelengths are absorbed much
157 faster than long wavelengths, therefore blue light penetrates much deeper into the water
158 column.⁴⁴ Non-spectral methods can overestimate PP by as much as 50% if only broadband
159 PAR is used.¹⁰ A number of calculations are necessary to spectrally resolve the glider
160 broadband PAR observations.

161

162 The glider only records subsurface PAR, so we first estimate surface irradiance for
163 comparison with a surface irradiance model. We then decompose the surface irradiance into
164 spectral components. Irradiance at depth was calculated using spectrally-weighted
165 algorithms.⁴⁶ Details are described below.

166

167 SG566 returned 1325 profiles of chlorophyll and PAR (downcast and upcast counted
168 separately). Profiles where PAR intensity increased with depth (due to passing cloud cover
169 and/or glider rolls)⁴⁶ were excluded from the analysis (319). We also excluded night-time
170 profiles (417) leaving a total of 589 simultaneous profiles for analysis.

171

172 *2.5.1 Estimating surface irradiance from subsurface glider measurements*

173 The fraction of solar irradiance entering the water column depends on the amount of sunlight
174 reflected by the sea surface. This is calculated by separating the diffuse and direct
175 components of irradiance using determinations of the Fresnel reflectance and the amount of
176 foam (see Supporting Information). The total reflectance (r_{tot}) is the sum of direct (r_d)
177 reflectance and diffusive reflectance (r_{diff}).

$$178 \quad r_{tot} = r_d + r_{diff} \quad [1]$$

179

180 Glider PAR was extrapolated to just below the surface by assuming exponential attenuation.

181 The following equation was then applied to calculate PAR just above the surface, $E(0^+)$

$$182 \quad E(0^+) = \frac{E(0^-)(1-R\bar{r})}{(1-r_{tot})} \quad [2]$$

183 where $E(0^-)$ is the irradiance just below the surface and R the irradiance reflectance (usually

184 < 0.1 in ocean waters). The water-air Fresnel reflection for the whole diffuse upwelling

185 radiation (\bar{r}) has a value of $0.48 R$ and \bar{r} are needed to obtain the upwelling irradiance

186 flux, which is subsequently reflected back down upon reaching the water surface.⁴⁴

187

188 *2.5.2. Calculating spectral irradiance*

189 Surface PAR from the Seaglider (Eq. 2) was spectrally decomposed into 5 nm wavelengths,

190 $E_0(\lambda)$, using a look-up table⁴¹ created by generating a clear sky run of a radiative transfer

191 model,⁴⁷ which is specific for oceanographic applications and adapted to include the effects

192 of cloud cover.⁴⁸ For a given day, this model is run for noon using the glider surfacing

193 position and relevant meteorological parameters to attenuate irradiance through the

194 atmosphere (British Atmospheric Data Centre, BADC). The model outputs a spectrally

195 resolved, full day irradiance time series just above the surface of the ocean for the location of

196 interest. The integrated irradiance over all wavelengths for the time of the glider

197 measurements was calculated in $\mu\text{mol quanta m}^{-2} \text{ s}^{-1}$. The ratio between $E(0^+)$ from Eq. 2

198 and the integrated clear sky run is used to scale the spectral values for the day in question

199 using each profile in that day to get spectral irradiance over the whole day at half hour

200 intervals.

201

202 *2.5.3. Spectral irradiance through the water column*

203 To calculate spectral irradiance ($E(z, \lambda)$) at a given depth in the water column we used the

204 equation,⁴⁹

205
$$E(z, \lambda) = E_0(\lambda) \int_z^0 \exp ([-K_w(\lambda) + K_c (\lambda)] z), \quad [3]$$

206 where $K_w(\lambda)$ is the attenuation coefficient associated with water and $K_c (\lambda)$ is the attenuation
207 coefficient associated with chlorophyll and other dissolved material at specific wavelengths,
208 λ . Morel et al.⁴⁵ calculate $K_c(\lambda)$ as

209
$$K_c(\lambda) = \chi_c(\lambda)Chl^{e(\lambda)}. \quad [4]$$

210 The coefficient χ_c and the exponent $e(\lambda)$ are both functions of wavelength and Chl is
211 chlorophyll concentration (mg m^{-3}). Wavelengths within the PAR broadband range are used
212 at 5 nm intervals.

213

214

215 **2.6. Chlorophyll Corrections and calibrations**

216 As the manufacturer's calibration is often insufficient^{20,50} a number of steps are carried out to
217 calibrate the chlorophyll estimates. First, the fluorescence data is corrected for quenching.
218 Second, a scale factor for chlorophyll-fluorescence is estimated by comparing modelled to
219 observed irradiance attenuation. Details are given below (Figure 1).

220

221 *2.6.1 Quenching Corrections*

222 Daytime chlorophyll fluorescence exhibited fluorescence quenching in the top 20 m with low
223 fluorescence during high irradiance. To correct for quenching we have used the night-time
224 relationship between fluorescence and optical backscatter (see Supporting Information for
225 details).^{38,51} We call the result the uncorrected-chlorophyll.

226

227 *2.6.2 PAR-based chlorophyll calibrated*

228 We calibrated the chlorophyll fluorescence sensor using the PAR measurements and Eq. (3)⁴⁹
229 to model the irradiance attenuation due to chlorophyll.⁴⁶ The uncorrected-chlorophyll profile

230 (with dives and climb treated separately) was divided by a scaling factor ranging from 0.2-25
231 in intervals of 0.2 and the spectral irradiance profile recalculated for each value based on the
232 resulting scaled chlorophyll concentration profile and surface irradiance (Eq. 3 and 4).
233 Modelled values of spectral irradiance were then integrated over all wavelengths (400-700
234 nm) to compare to glider PAR measurements. A root mean squared error (RMSE) was
235 calculated between the modelled and measured PAR values, over all depths (typically 50
236 points), for each scale factor.

237

238 For each profile the scale factor with the lowest RMSE was then used to scale the
239 uncorrected-chlorophyll concentration. This approach produces an independent scaling factor
240 for each dive/climb, allowing for drift in the fluorometer to be corrected. The method
241 assumes Case I water characteristics where CDOM and particulates co-vary with
242 phytoplankton.^{51,52} This method can be used if the glider PAR sensor is uncalibrated provided
243 the fluorescence-chlorophyll relationship is linear as we are only calculating attenuation
244 rather than absolute PAR.

245

246 Variation in the scaling factor over a deployment period may result from poorly resolved
247 PAR profiles (e.g. significant glider rolls or cloud cover). Profile-to-profile variability was
248 reduced by using the median scaling factor calculated for a 10-day moving window. A 10-
249 day window was picked arbitrarily, but no significant difference was seen using 6, 8 or 10
250 days. Longer time intervals resulted in over-smoothing of the scaling factor.

251

252 Final PAR-corrected chlorophyll concentrations for each profile were obtained using the
253 appropriate 10-day median scale factor (Figure 2). These calibrated chlorophyll profiles

254 (Figure 3) were used as input into the PP model, along with the spectral downwelling PAR
255 (Section 3.1).

256

257 **2.7. Calculating Primary Production**

258 PP was calculated with the glider profiles of irradiance and PAR-corrected chlorophyll using
259 depth, time and wavelength-resolved irradiance.⁴² PP is represented by a triple integral,
260 integrating over day length (L), depth (D) and wavelength λ from $\lambda_1=400\text{nm}$ to $\lambda_2=700\text{ nm}$,

261

$$262 \quad PP = 12 \int_0^L \int_0^D \int_{\lambda_2}^{\lambda_1} Chl(Z) PAR(\lambda, Z, t) a^*(\lambda) \phi_{\mu}(\lambda, Z, t) d\lambda dZ dt \quad [5]$$

263 where a^* is the absorption cross section per unit of chlorophyll (m^{-1}), ϕ_{μ} is the net growth
264 rate ($\text{mol C (mol quanta)}^{-1}$). These values are parameterised as in Morel et al. (1996, see
265 Supporting Information for details).⁵⁴ Each separate dive and climb were assigned an average
266 time and position (latitude and longitude) for the profile. The model requires surface
267 downwelling spectral irradiance ($\text{Wm}^{-2} \text{ nm}^{-1}$), which is provided by the glider PAR sensor
268 (Section 3.1.3.).

269

270 **3. Results**

271 **3.1 Glider chlorophyll**

272 *3.1.1. PAR-Corrected Chlorophyll data*

273 The scale factor used to calibrate the chlorophyll data (Figure 2) has a mean of 3 (range 0.6 –
274 11). In May there is a peak of 5 but only 4 profiles were used to calculate this scale factor
275 (range 1.2-8.8), as the sensors were turned off for a time to save battery, so it is not as well
276 constrained as in other months when more profiles were available. Starting in July the scale
277 factor was less variable (range 1.2 - 1.8) for the remainder of the deployment.

278

279 The chlorophyll profiles are shown in Figure 3 for the whole deployment period.
280 Concentrations were $<1.5 \text{ mg Chl-}a \text{ m}^{-3}$ from May until July, when they increased to $>2 \text{ mg}$
281 $\text{Chl-}a \text{ m}^{-3}$. Before July the chlorophyll concentration varied little within the top 30 m. A SCM
282 started to form towards the end of July, with maximum chlorophyll concentrations $>4 \text{ mg}$
283 $\text{Chl-}a \text{ m}^{-3}$ at a depth of 30 m. Surface concentrations during August were very low, $<0.6 \text{ mg}$
284 $\text{Chl-}a \text{ m}^{-3}$. By the end of August the SCM deepened to 40 m and maximum concentrations in
285 the SCM decreased to $<2.5 \text{ mg Chl-}a \text{ m}^{-3}$, with surface concentrations $<0.4 \text{ mg Chl-}a \text{ m}^{-3}$.

286

287 *3.1.2 Comparison of glider and bottle-sample estimates of chlorophyll*

288 Figure 4 compares discrete bottle-sample chlorophyll and PAR-corrected glider chlorophyll
289 for the 3 cruises. In late April (JC085) and prior to the spring bloom, the discrete chlorophyll
290 concentrations were comparable to the PAR-corrected chlorophyll concentrations. Surface
291 concentrations ranged from $0.25 - 0.7 \text{ mg Chl-}a \text{ m}^{-3}$ and $0.15 - 0.8 \text{ mg Chl-}a \text{ m}^{-3}$ for the
292 discrete samples and glider estimates, respectively. The range in glider-based chlorophyll
293 concentrations was slightly larger; likely due to the greater number of glider profiles
294 detecting a wider range of concentrations. At depths between 75 - 150 m, bottle samples were
295 approximately $0.1 - 0.2 \text{ mg Chl-}a \text{ m}^{-3}$ higher than the glider, which effectively measured
296 close to zero at these depths, which is below the euphotic depth (60 m).

297

298 In June the majority of discrete chlorophyll measurements were elevated compared to the
299 glider estimates, particularly throughout the upper 50 m. Surface concentrations ranged from
300 $0.05 - 1.2 \text{ mg Chl-}a \text{ m}^{-3}$ for the glider compared with $0.08 - 1.8 \text{ mg Chl-}a \text{ m}^{-3}$ from bottle
301 samples (Figure 4). There was no offset between the glider and discrete measurements below
302 75-150 m, suggesting no systematic error. Chlorophyll values below 100 m were $<0.4 \text{ mg}$
303 $\text{Chl-}a \text{ m}^{-3}$, with the majority of the glider and discrete measurements $<0.2 \text{ mg Chl-}a \text{ m}^{-3}$.

304

305 For the final cruise in September (JC90) discrete and glider chlorophyll estimates were
306 comparable (Figure 4). Surface values ranged between 0.4 and 1 mg Chl-*a* m⁻³ in the discrete
307 water samples, whereas the glider chlorophyll ranged from <0.1 to 0.75 mg Chl-*a* m⁻³. A
308 SCM around 40 m was measured by both data sets, with similar maximum values (3.3 mg
309 Chl-*a* m⁻³).

310

311 The lateral distances between CTD and glider profiles were compared with the differences in
312 surface chlorophyll concentrations (Figure S4, Supporting Information, Spearman⁵⁵ $R^2 =$
313 0.53, $p < 0.001$, $n = 19$). Surface chlorophyll differences decrease with distance, suggesting
314 that spatial differences remain an important consideration in the comparison of glider and in
315 situ data. Many of the CTD profiles were located >30 km away from the glider making it
316 possible that spatial variability associated with the onset of the spring bloom at this time
317 affects the comparison. This is also consistent with the glider data, which can show
318 significant variations in water mass properties and chlorophyll concentrations along a single
319 15-km transect. Cloud cover hinders examining this from satellite images in more detail.

320

321

322 **3.2 Depth Integrated Primary Production**

323 *3.2.1 Depth integrated glider estimates of primary production*

324 Glider based estimates of PP ranged from 0.38 to 30 g C m⁻² d⁻¹ over the 5 months, displaying
325 strong temporal variability. These estimates have been compared to ship-based ¹³C
326 measurements and 1 km satellite estimates (Figure 5).

327

328 The ^{13}C PP estimates from June are compared to glider estimates in Figure 5a. Glider profiles
329 on the same day were averaged together for comparison. ^{13}C PP increased from 6th to 14th
330 June, with values ranging from 0.5 – 1.9 g C m⁻² d⁻¹, whereas the glider estimates of PP were
331 relatively consistent, varying from 1.1 to 1.6 g C m⁻² d⁻¹ over the same time period. Glider PP
332 measurements were higher on average by 0.17 g C m⁻² d⁻¹ (or 39%) but offsets were also
333 highly variable (Figure 5a).

334

335 PP estimates obtained using the uncorrected-chlorophyll profiles are also presented in Figure
336 5a. On average this resulted in productivity estimates over two fold higher than the ^{13}C
337 observations.

338

339 In Figure 5b we present a time series of water column integrated PP over the five month
340 glider deployment, in conjunction with ^{13}C measurements already shown in Figure 5a. The
341 glider estimates were higher than the ^{13}C measurements but not unreasonably so. Integrated
342 PP rates from late April to May were ~ 1 g C m⁻² d⁻¹ increasing to a maximum of 3 g C m⁻² d⁻¹
343 in July. Towards the end of July and through August rates decreased to 1.5 g C m⁻² d⁻¹ but
344 remained highly variable, fluctuating by ± 0.6 g C m⁻² d⁻¹. Due to the high level of cloud
345 cover there were no satellite pixel matches during the time period when the in situ
346 measurements were taken and therefore a comparison with satellite and ship-based
347 measurements was not possible.

348

349 Integrated PP estimates from the glider and satellite were also compared (section 2.3, Figure
350 5c). The correlation between the satellite and glider estimates of surface PP was modest but
351 nevertheless statistically significant (Figure S5, Supporting Information; Spearman⁵⁵, $R^2 =$
352 0.322, $P < 0.0001$, $n=122$). In general the glider shows higher integrated estimates of PP than

353 the satellite. Dissimilarity between estimates is likely due to differences in the PAR values
354 and between the modelled and observed SCM. The mean root mean squared error between
355 the modelled and observed chlorophyll profiles was 0.9 mg Chl-*a* m⁻³ (range 0.58–1.36 mg
356 Chl-*a* m⁻³).

357

358 Figure 5c shows that the satellite and glider have reasonably good agreement during the
359 deployment with similar variability, trends and magnitude in PP. Both datasets show an
360 increase in production from May to June (spring bloom) and a production maximum in July,
361 with maximum rates of 3 and 2 g C m⁻² d⁻¹ decreasing again in late July; for the glider and
362 satellite respectively. Although glider estimates of PP are on average 16% higher than
363 satellite estimates.

364

365 *3.2.2 Glider estimates of seasonal primary production vs literature estimates*

366 Due to the limited number of ¹³C in situ measurements we also present a comparison with
367 productivity estimates from the literature for the same region (Table 1).^{25,56-59} The literature
368 values span 0.3 – 2 g C m⁻² d⁻¹, comparable with our ¹³C measurements. However, towards
369 the end of June and July the literature observations are lower than those estimated from the
370 glider and our ¹³C measurements. This may be inter-annual variability. Overall our ¹³C values
371 are within the range of literature values supporting the use of this data to compare to the
372 glider estimates.

373

374 **3.3 Depth resolved primary production**

375 Depth resolved PP over the deployment (Figure 6) shows that throughout May and June PP
376 was highest at the surface and decreased with depth due to irradiance attenuation. In July, as

377 chlorophyll and irradiance concentrations increased PP also increased with maximum surface
378 rates of $0.45 \text{ g C m}^{-3} \text{ d}^{-1}$. In late July a subsurface production maximum formed with PP rates
379 of $0.2 - 0.3 \text{ g C m}^{-3} \text{ d}^{-1}$. The production maximum deepened throughout August from 15 to 30
380 m. The productivity maximum was located just beneath the mixed layer but also below the
381 optical sampling depth for remote sensing.

382

383 The euphotic depth was 60-80 m throughout May and June, with variable mixed layer depths
384 (MLD) of between 40 and 130 m. The euphotic depth shoaled to 35 m in July coincident with
385 increasing chlorophyll concentrations and greater irradiance attenuation⁵³ and a shoaling of
386 the MLD due to either surface forcing (heating) or a re-stratification through physical
387 processes such as Ekman transport, mixed layer instabilities and lateral advection. The
388 subsurface production maximum in late July and August was around the same depth as the
389 mixed layer. However the SCM was deeper by 10 m than the production maximum, and
390 below the mixed layer, suggesting that the SCM was preferentially located where nutrient
391 concentrations were higher. In August the SCM was located between the MLD and the
392 euphotic depth (Figure 3).

393

394 Depth profiles of the ^{13}C productivity measurements are shown in Figure S6 (Supporting
395 Information) alongside the range and mean of the coincident glider profiles. Although the ^{13}C
396 productivity rates were lower than the mean glider profile, they lie mostly within the range of
397 glider data. Some of the ^{13}C profiles show a production maximum around 30 m whereas the
398 glider estimated profiles do not. Two profiles also show higher production at depth than
399 estimated from the glider.

400

401 **4. Discussion**

402 **4.1 Advantages of calculating Primary Production using gliders**

403 Fine scale measurements are important since submesoscale features are often present, such as
404 highly productive filaments.²⁵ Furthermore, PP may change over daily time scales due to
405 changes in irradiance and mixed layer depth. Such short timescales (hours) are not resolved
406 by remote sensing, but with several profiles a day a glider can observe these changes. Early
407 June showed differences in integrated production rates between sequential dives of between
408 0.3 and 1 g C m⁻² d⁻¹. The average daily production was <2 g C m⁻² d⁻¹, so this difference was
409 significant. Small scale temporal variations in PP may be important in determining the carbon
410 budget,²⁵ especially in areas of high variability of phytoplankton.

411

412 A key advantage of using gliders is the ability to resolve subsurface features, previously only
413 possible using ship-based measurements. Satellite production estimates are only resolved to
414 the first optical depth and it has been shown that including fluorescence profiles significantly
415 improves estimates.¹² Knowing the distribution of chlorophyll at depth is considered vital for
416 ecological studies.⁶⁰ Glider production rates were 16% higher than satellite estimates during
417 the deployment suggesting that satellite-based estimates of production may be slightly
418 underestimating PP during summer months in this region. Subsurface chlorophyll maxima
419 contribute significantly to integrated PP in temperate latitudes so implementation of
420 subsurface glider profiles will improve regional estimates.⁶¹ Subsurface production maxima
421 are common globally and this contribution is often modelled incorrectly for specific regions
422 when using satellite colour to estimate PP.^{15,62,63} Therefore gliders have considerable
423 potential to improve satellite estimates of PP.¹²

424

425 Gliders also have the benefit of being able to continuously sample in all weather conditions.
426 Ship-based measurements are weather and time dependent. Satellite coverage is restricted by

427 cloud cover, which can introduce sampling bias.^{64,65} During this deployment 467 profiles out
428 of 589 (79 %) had no direct satellite matchup due to high levels of cloud cover, equating to a
429 loss of 105 days of satellite coverage over the whole deployment of 141 days. Using 1 km
430 pixel match ups is a strong constraint impacting the number of match-ups.

431

432

433 **4.2 Limitations of glider estimated primary production**

434 The spectral constants for chlorophyll used in the irradiance attenuation calculations (Eq. 4),
435 differ compared to other literature values due to regional differences in community
436 composition and/or temperature.^{66,67} Additional uncertainty is introduced when broadband
437 PAR is split spectrally. The method assumes that clouds, changes in atmospheric absorption
438 and season, influence spectral values of PAR linearly.⁴¹ The photosynthetic rate per unit of
439 biomass (Eq. 5) remains the largest unknown in the PP algorithm because of its high
440 variability in the ocean.⁶⁸

441

442 Fluorescence measurements, which are only a proxy for chlorophyll-*a*, can be difficult to
443 interpret. The fluorescence yield per unit of chlorophyll is known to change in response to
444 changes in community structure.⁶⁹ The changing scale factor used to calibrate glider
445 chlorophyll and the rapid decrease in the scale factor seen in July (Figure 2) may therefore be
446 indicative of post bloom changes to the community composition. We cannot verify this with
447 the data available. However, using a time-dependent scale factor to probe community
448 structure would be interesting topic to explore.

449

450 Measurements from autonomous platforms present their own challenges. Sensor calibrations
451 may drift with time or with biofouling.¹⁸ Additional calibration measurements collected at

452 deployment and recovery could indicate this. For this deployment no biofouling was noted at
453 recovery and there was no drift in dark counts at depth, so fouling is unlikely. Discrepancies
454 were seen between bottle data and the PAR-corrected glider chlorophyll. As few CTD casts
455 were made near the glider and this area is known to display patchy chlorophyll
456 distributions,²⁵ comparisons can be complicated. However the data are broadly consistent
457 suggesting that glider productivity rates are generally appropriate for the region.

458

459 **4.3 Future applications**

460 While we have used gliders to quantify PP in a region of the North Atlantic, this approach
461 will allow improved estimates of PP more widely in the future, particularly in regions with
462 SCMs and/or considerable cloud cover. We have demonstrated the suitability of gliders for
463 capturing fine-scale temporal changes in production at daily timescales over a single season.
464 Gliders allow coincident and simultaneous measurements of physical parameters, including
465 density, temperature, oxygen and vertical water velocity.^{70,71} The coincident analysis of the
466 physical environment allows an improved understanding of influences on phytoplankton
467 growth. Small-scale physical processes may account for a significant amount of new
468 production.^{50,72-73} Several recent studies have used high resolution data from gliders to
469 analyse biological and physical connections.⁷⁴⁻⁷⁶ Simultaneous estimates of PP will further
470 resolve biological and physical connections.

471

472

473

474

475

476

477

478 **Acknowledgements**

479 Funding was provided by the Natural Environmental Research Council (NERC) through the
480 Sensors on Gliders program GliSENE_x (NE/J020184/1), the Ocean Surface Boundary Layer
481 (OSMOSIS) project (NE/I020083/1), NERC National Capability (cruises JC85, JC87).
482 Additional funding was provided by EU Framework 7 project EuroBASIN (FP7-ENV-2010;
483 cruise JC87) and the National Science Foundation (OCE1155676). We would like to thank
484 the captains and crew aboard the RRS James Cook. ECMWF Operational Analyses were
485 obtained by Tim Smyth from the British Atmospheric Data Centre. The authors thank the
486 NERC Earth Observation Data Acquisition and Analysis Service (NEODAAS) for supplying
487 data for this study.

488

489 **Additional Content**

490 **Supporting Information**

491 Extended Methods, specifically quenching corrections, validation of PAR and surface
492 irradiance calculations and Figures S1-S6. This material is available free of charge via the
493 Internet at <http://pubs.acs.org>

494

495 **References**

- 496 1 Carr, M. E.; Friedrichs M. A. M.; Schmeltz, M.; Aita, M. N.; Antoine, D.; Arrigo, K. R.;
497 Asanuma, I.; Aumont, O.; Barber, R.; Behrenfeld, M.; Bidigare, R.; Buitenhuis, E. T.;
498 Campbell, J.; Ciotti, A.; Dierssen, H.; Dowell, M.; Dunne, J.; Esaias, W.; Gentili, B.;
499 Gregg, W.; Groom, S.; Hoepffner, N.; Ishizaka, J.; Kameda, T.; Le Quéré, C.;
500 Lohrenz, S.; Marra, J.; Mélin, F.; Moore, K.; Morel, A.; Reddy, T. E.; Ryan, J.;
501 Scardi, M.; Smyth, T.; Turpie, K.; Tilstone, G.; Waters, K.; Yamaznaka, Y. A
502 comparison of global estimates of marine primary production from ocean color. *Deep*
503 *Sea Research Part II*, **2006**, 53 (5-7), 741–770; DOI:10.1016/j.dsr2.2006.01.028
- 504 2 Field, C. B. Primary Production of the Biosphere: Integrating Terrestrial and Oceanic
505 Components. *Science*, **1998**. 281 (5374), 237–240; DOI:10.1126/science.281.5374.237
- 506 3 Parekh, P.; Follows, M.J.; Dutkiewicz, S.; Ito, T. Physical and biological regulation of the
507 soft tissue carbon pump. *Paleoceanography*, **2006**, 21, PA3001;
508 DOI:10.1029/2005PA001258.
- 509 4 Nightingale, P.D.; Malin, G.; Law, C.S.; Watson, A.J.; Liss, P.S.; Liddicoat, M.J.; Boutin,
510 J.; Upstill-Goddard, R.C. In situ evaluation of air-sea gas exchange parameterizations
511 using novel conservative and volatile tracers. *Global Biogeochemical Cycles*, **2000**, 14
512 (1), 373-387.
- 513 5 Wanninkhof, R. Relationship between wind speed and gas exchange over the ocean. *J.*
514 *Geophys. Res.*, **1992**, 97 (C5), 7373-7382.

- 515 6 Liss, P.S.; Merlivat, L. Air-sea gas exchange rates: introduction and synthesis, in The Role
516 of Air-Sea Exchange in Geochemical Cycling, edited by P. Buat-Ménart, 113-129, D.
517 Reidel, Hingham, Mass, 1986.
- 518 7 Eppley, R.W.; Stewart, E.; Abbott, M.R.; Heyman, U. Estimating ocean production from
519 satellite chlorophyll: introduction to regional difference and statistics in the southern
520 California bight. *Journal of Plankton Research*, **1985**, 7 (1), 57-70;
521 DOI: 10.1093/plankt/7.1.57
- 522 8 Bidigare, R.R.; Smith, R. C.; Baker, K. S.; Marra, J. Oceanic primary production estimates
523 from measurements of spectral irradiance and pigment concentrations, *Global*
524 *Biogeochemical Cycles*, **1987**, 1 (3), 171-186
- 525 9 Platt, T.; Sathyendranath, S. Oceanic primary production: estimation by remote sensing at
526 local and regional scales. *Science*, **1988**, 241 (4873), 1613-1620.
527 DOI:10.1126/science.241.4873.1613
- 528 10 Sathyendranath, S.; Platt, T.; Caverhill, C.; Warnock, R.; Lewis, M. Remote sensing of
529 oceanic primary production: computations using a spectral model. *Deep Sea*
530 *Research*, **1989**, 36(3), 431-453; DOI:10.1016/0198-0149(89)90046-0
- 531 11 Behrenfeld, M. J.; Falkowski, P. G. A consumer's guide to phytoplankton primary
532 productivity models, *Limnology and Oceanography*, **1997**, 42, 1479-1491.
- 533 12 Jacox, M.G.; Edwards, C.; Kahru, M.; Rudnick, .D.L.; Kudela, R.M. The potential for
534 improving remote primary productivity estimates through subsurface chlorophyll and
535 irradiance measurement. *Deep Sea Research Part II*, **2015**, 112, 107-116;
536 DOI:10.1016/j.dsr2.2013.12.008

- 537 13 Gordon, H.R.; Clark, K. Remote sensing optical properties of a stratified ocean: an
538 improved interpretation. *Applied Optics*, **1980**, *19* (20), 3428-3430;
539 DOI:10.1364/AO.19.003428.
- 540 14 Morel A.; Berthon, J. Surface pigments, algal biomass profiles and potential production of
541 the euphotic layer: relationships reinvestigated in view of remote-sensing applications.
542 *Limnology and Oceanography*, **1989**, *34*, 1545-1562.
- 543 15 Cullen J.J. Subsurface chlorophyll maximum layers: enduring enigma or mystery solved.
544 *Annual Review of Marine Science*, **2015**, *7*, 207-239; DOI: 10.1146/annurev-marine-
545 010213-135111.
- 546 16 Eriksen, C. C.; Perry, M.J., "The Nurturing of Seagliders By the National Oceanographic
547 Partnership Program". School of Marine Sciences at DigitalCommons@UMaine.Marine
548 Sciences Faculty Scholarship. **2009**, Paper 133
- 549 17 Rudnick, D. L.; Cole, S.T. On sampling the ocean using underwater gliders. *J. Geophys.*
550 *Res.*, **2011**, *116*, C08010; DOI:[10.1029/2010JC006849](https://doi.org/10.1029/2010JC006849).
- 551 18 Perry, M.J.; Sackmann, B.S.; Eriksen, C.C.; Lee, C.M. Seaglider observations of blooms
552 and subsurface chlorophyll maxima off the Washinton coast. *Limnology and*
553 *Oceanography*, **2008**, *53* (5, part 2), 2169-2179; DOI:
554 10.4319/lo.2008.53.5_part_2.2169
- 555 19 Lorenzen, C.J. A method for the continuous measurement of in vivo chlorophyll
556 concentration. *Deep Sea Research*, **1966**, *13*, 223-227.

- 557 20 Mignot, A.; Claustre, H.; D'Ortenzio, F.; Xing, X.; Poteau, A.; Ras., J. From the shape of
558 the vertical profile of in vivo fluorescence to Chlorophyll-a concentration.
559 *Biogeosciences*, **2011**, *8*, 2391–2406
- 560 21 Lampitt, R. S.; Favali, P.; Barnes, C. R.; Church, M. J.; Cronin, M. F.; Hill, K.
561 L.; Kaneda, Y.; Karl, D. M.; Knap, A. H.; McPhaden, M. J. Nittis, K. A.; Priede, I.
562 G.; Rollin, J-F.; Send, U.; Teng, C-C.; Trull, T. W.; Wallace, D.W. R.; Weller, R. A. In
563 situ sustained Eulerian observatories. In, Hall, J., Harrison, D.E. and Stammer,
564 D. (eds.) *Proceedings of OceanObs'09: Sustained Ocean Observations and Information*
565 *for Society, Vol. 1. OceanObs'09: Sustained Ocean Observations and Information for*
566 *Society* Noordwijk, The Netherlands, European Space Agency, **2010**, 395-404. (ESA
567 Special Publication WPP-306).
- 568
- 569 22 Hartman, S. E.; Lampitt, R. S.; Larkin, K. E.; Pagnani, M.; Campbell, J.; Gkritzalis, T.;
570 Jiang, Z-P.; Pebody, C. A.; Ruhl, H. A.; Gooday, A. J.; Bett, B. J.; Billett, D. S. M.;
571 Provost, P.; McLachlan, R.; Turton, J. D.; Lankester, S. The Porcupine Abyssal Plain
572 fixed-point sustained observatory (PAP-SO): variations and trends from the Northeast
573 Atlantic fixed=point time-series. *ICES Journal of Marine Science*, **2012**, *69* (5), 776-
574 783; DOI:10.1093/icesjms/fss077
- 575 23 Lampitt, R. S.; Bett, B. J.; Kiriakoulis, K.; Popova, E. E.; Ragueneau, O.; Vangriesheim,
576 A.; Wolff, G. A. Material supply to the abyssal seafloor in the Northeast Atlantic.
577 *Progress in Oceanography*, **2010**, *50*, 27-63.
- 578 24 Hartman, S. E.; Larkin, K. E.; Lampitt, R. S.; Lankhorst, M.; Hydes, D.J. Seasonal and
579 inter-annual biogeochemical variations in the Porcupine Abyssal Plain 2003-2005

580 associateds with winter mixing and surface circulation. *Deep Sea Research Part II*,
581 **2010**, 57 (15), 1303-1312; DOI:10.1016/j.dsr2.2010.01.007

582 25 Painter, S. C.; Pidcock, R. E.; Allen, J. T. A mesoscale eddy driving spatial and temporal
583 heterogeneity in the productivity of the euphotic zone of the northeast Atlantic. *Deep*
584 *Sea Research Part II*, **2010**, 57 (15), 1281-1292; DOI: 10.1016/j.dsr2.2010.01.005

585 26 Barlow, R. G.; Mantoura, R. F. C.; Gough, M. A.; Fileman, T. W. Pigment signatures of
586 phytoplanktoncomposition in the northeast Atlantic during the 1990 spring bloom.
587 *Deep-Sea Research II*, **1993**, 40 (1/2), 459-477.

588 27 Henson, S.; Lampitt, R.; Johns, D. Variability in phytoplankton community structure in
589 response to the North Atlantic Oscillation and implications for organic carbon flux.
590 *Limnology and Oceanography*, **2012**, 57 (6), 1591-1601;
591 DOI:10.4319/lo.2012.57.6.1591.

592 28 Lochte, K.; O. Pfannkuche, O. Cyclonic cold-core eddy in the eastern North Atlantic. II.
593 Nutrients, phytoplankton and bacterioplankton. *Marine Ecology Progress Series*,
594 **1987**, 39, 153-164.

595 29 Painter, S. C.; Lucas, M. I.; Stinchcombe, M. C.; Bibby, T. S.; Poulton, A. J. Summertime
596 trends in pelagic biogeochemistry at the Porcupine Abyssal Plain study site in the
597 nothereast Atlantic. *Deep Sea Research Part II*, **2010**, 57 (15), 1313-1323;
598 DOI:10.1016/j.dsr2.2010.01.008

599 30 Smythe-Wright, D.; Boswell, S.; Kim, Y-N.; Kemp, A. Spatio-temporal changes in the
600 distribution of phytopigments and phytoplanktonicgroups at the Porcupine Abyssal

601 Plain (PAP) site. *Deep Sea Research Part II*, **2010**, 57 (15), 1324-1335.
602 doi:10.1016/j.dsr2.2010.01.009

603 31 Eriksen, C. C.; Osse, T. J.; Light, R. D.; Wen, T.; Lehman, T. W.; Sabin, P. L.; Chiodi, M.
604 Seaglider: a long-range autonomous underwater vehicle for oceanographic research.
605 *IEEE Journal of Oceanic Engineering*, **2001**, 26 (4), 424–436. doi:10.1109/48.972073

606 32 Rudnick, D. L.; Davis, R. E.; Eriksen, C. C.; Fratantoni, D. M.; Perry, M. J. Underwater
607 Gliders for Ocean Research. *Marine Technology Society Journal*, **2004**, 37 (2) 73-84;
608 DOI:10.4031/002533204787522703.

609 33 Davis, R. E.; Eriksen, C. C.; Jones, C. P. Autonomous Buoyancy-Driven Underwater
610 Gliders. In G. Griffiths, editor, *The Technology and Applications of Autonomous*
611 *Underwater Vehicles*. Taylor and Francis, London, U.K., 2002.

612 34 Garau, B.; Ruiz, S.; Zhang, W. G.; Pascual, A.; Heslop, E.; Kerfoot, J.; Tintoré, J.
613 Thermal lag correction on Slocum CTD glider data. *Journal of Atmospheric and*
614 *Oceanic Technology*, **2011**, 28 (9), 1065-1071.

615 35 Damerell, G. M.; Heywood, K. J.; Thompson, A. F. Ocean Glider Observations of the
616 Seasonal Evolution of the Upper Ocean in the north-east Atlantic. *Geophys. Res. Lett.*,
617 in preparation.

618 36 Wetlabs ECO fluorometers and scattering sensors, User Manual 10/2014 Edition 4.
619 <http://wetlabs.com/sites/default/files/documents/WETLabs-ECOMaster=3en.pdf>

620 37 Stramski, D.; Boss, E.; Bogucki, D.; Voss, K. J. The role of seawater constituents in light
621 backscattering in the ocean. *Progress in Oceanography*, **2004**, 61, 27-56;
622 DOI:10.1016/j.pocean.2004.07.001

- 623 38 Welschmeyer, N. Fluorometric analysis of chlorophyll a in the presence of chlorophyll b
624 and pheopigments. *Limnology and Oceanography*, **1994**, 39 (8), 1985–1992;
625 DOI:10.4319/lo.1994.39.8.1985
- 626 39 Slawyk, G.; Collos, Y.; Auclair, J.C. The use of the ¹³C and ¹⁵N isotopes for the
627 simultaneous measurement of carbon and nitrogen turnover rates in marine
628 phytoplankton. *Limnology and Oceanography*, **1977**, 22, 925-932.
- 629 40 Legendre, L.; Gosselin, M., 1996: Estimation of N and C uptakes rates by phytoplankton
630 using ¹⁵N and ¹³C: revisiting the usual computation formulae. *Journal of Plankton*
631 *Research*, **1996**, 19 (2), 263-271.
- 632 41 Smyth, T. J.; Tilstone, G. H.; Groom, S. B. Integration of radiative transfer into satellite
633 models of ocean primary production. *J. Geophys. Res.*, **2005**, 110 (C10), C10014;
634 DOI:10.1029/2004JC002784
- 635 42 Morel, A. Light and marine photosynthesis : a spectral model with geochemical and
636 climatological implications. *Progress in Oceanography*, **1991**, 26, 263–306;
637 DOI:10.1016/0079-6611(91)90004-6
- 638 43 Mobley, C. D. Hydrolight 3.0 Users' Guide. SRI International, Menlo Park, California,
639 U.S.A., **1995**.
- 640 44 Kirk, J. T. O. Light and Photosynthesis in Aquatic Ecosystems, Cambridge University
641 Press, Cambridge, U.K., 2011.
- 642 45 Morel, A.; Maritorena, S. Bio-optical properties of oceanic waters: A reappraisal. *J.*
643 *Geophys. Res.*, **2001**, 106 (C4), 7163–7180; DOI:10.1029/2000JC000319.

644 46 Xing, X.; Morel, A.; Clausre, H.; Antoine, D.; D'Ortenzio, F.; Poteau, A.; Mignot, A.
645 Combined processing and mutual interpretation of radiometry and fluorimetry from
646 autonomous profiling Bio-Argo floats: Chlorophyll a retrieval. *J. Geophys. Res.*, **2011**,
647 *116*, C06020; DOI:10.1029/2010JC006899.

648 47 Gregg, W.; Carder, K. A simple spectral solar irradiance model for cloudless maritime
649 atmospheres. *Limnology*, **1990**, *35* (8), 1657–1675.

650 48 Reed, R. K. On estimating insolation over the ocean. *Journal of Physical Oceanography*,
651 **1977**, *7*, 482-485.

652 49 Carr, M.R. Modelling the Attenuation of Broad Band Light Down a Water Column.
653 *Journal of the Royal Statistical Society, Series D (The Statistician)*, **1986**, *35* (3), 325-
654 33; DOI:10.2307/2987748.

655 50 Frajka-Williams, E.; Rhines, P. B.; Eriksen, C. Physical controls and Mesoscale variability
656 in the Labrador Sea spring phytoplankton bloom observed by Seaglider. *Deep-Sea*
657 *Research I*, **2009**, *56*, 2144-2161; DOI:10.1016/j.dsr.2009.07.008

658 51 Boss, E.; Swift, D.; Taylor, L.; Brickley, P.; Zaneveld, R.; Riser, S.; Perry, M.J. Robotic in
659 situ and satellite- based observations of pigment and particle distributions in the Western
660 North Atlantic. *Limnology and Oceanography*, **2008**, *53*, 2112-2122;
661 DOI:10.4319/lo.2008.53.5_part_2.2112

662 52 Morel, A. Optical modelling of the upper ocean in relation to its biogenous matter content
663 (case 1 water). *J. Geophys. Res.*, **1988**, *93* (C9), 10749-10769;
664 DOI: 10.1029/JC093iC09p1074953

- 665 53 Bricaud, A.; Morel, A.; Babin, M.; Allali, K.; Claustre, H. Variations of light absorption
666 by suspended particles with chlorophyll a concentration in oceanic (case 1) waters:
667 Analysis and implications for bio-optical models. *J. Geophys. Res.*, **1998**, *103*, 31,033–
668 031,044.
- 669 54 Morel, A.; Antoine, D.; Babin, M.; Dandonneau, Y. Measured and modelled primary
670 production in the northeast Atlantic (EUMELI JGOFS program): the impact of natural
671 variations in the photosynthetic parameters on model predictive skill. *Deep-Sea*
672 *Research*, **1996**, *43* (8), 1273-1304.
- 673 55 Spearman C. The proof and measurement of association between two things. *Amer. J.*
674 *Psychol.* **1904**, *15*, 72–101; DOI:10.2307/1412159.
- 675 56 Chipman, D.W.; Marra, J.; Takahashi, T. Primary production at 47°N and 20°W in the
676 North Atlantic Ocean: a comparison between the ¹⁴C incubation method and mixed
677 layer carbon budget. *Deep Sea Research Part II*, **1993**, *40*, 151-169;
678 DOI:10.1016/0967-0645(93)90011-B
- 679 57 Marra, J.; Langdon, C.; Knudson, C. A. Primary production, water column changes, and
680 the demise of a *Phaeocystis* bloom at the Marine Light-Mixed Layers site (59° N, 21°
681 W) in the northeast Atlantic Ocean. *J. Geophys. Res.*, **1995**, *100* (C4), 6633-6643.
- 682 58 Savidge, G.; Boyd, P.; Pomroy, A.; Harbour, D.; Joint, I. Phytoplankton production and
683 biomass estimates in the northeast Atlantic Ocean, May–June 1990. *Deep Sea Research*
684 *Part I*, **1995**, *42* (5), 599-617.
- 685 59 Bury, S. J.; Boyd, P. W.; Preston, T.; Savidge, G.; Owens, N. J. P. Size-fractionated
686 primary production and nitrogen uptake during a North Atlantic phytoplankton bloom:

687 implications for carbon export estimates. *Deep Sea Research Part I*, **2001**, 48 (3), 689-
688 720.

689 60 Uitz, J.; Claustre, H.; Morel, A.; Hooker, S.B. Vertical distribution of phytoplankton
690 communities in open ocean: An assessment based on surface chlorophyll. *J. Geophys.*
691 *Res.*, **2006**, 111, C08005; DOI:10.1029/2005JC003207.

692 61 Anderson, G.C. Subsurface chlorophyll maximum in the northeast Pacific Ocean.
693 *Limnology and Oceanography*, **1969**, 14, 386-391.

694 62 Weston, K.; Fernand, L.; Mills, D.K.; Delahunty, R.; Brown, J. Primary production in the
695 deep chlorophyll maximum of the central North Sea. *Journal of Plankton Research*,
696 **2005**, 27 (9), 909-922; DOI: 10.1093/plankt/fbi064

697 63 Martin, J.; Tremblay, J.; Gagnon, J.; Tremblay, G.; Lapoussière, A.; Jose, C.; Poulin, M.;
698 Gosselin, M.; Gratton, Y.; Michel, C. Prevalence, structure and properties of subsurface
699 chlorophyll maxima in Canadian Arctic waters. *Marine Ecology Progress Series*, **2010**,
700 412, 69-84; DOI:10.3354/meps08666

701 64 Longhurst, A.; Sathyenranath, S.; Platt, T.; Caverhill C. An estimate of global primary
702 production in the ocean from satellite radiometer data. *Journal of Plankton Research*,
703 **1995**, 17 (6), 1245-1271; DOI:10.1093/plankt/17.6.1245

704 65 Gregg, W. W.; Casey, N. W. Sampling biases in MODIS and SeaWiFS ocean chlorophyll
705 data. *Remote Sensing of Environment*, **2007**, 111 (1), 25-35;
706 DOI:10.1016/j.rse.2007.03.008

707 66 Carder, K. L.; Chen, F. R.; Lee, Z. P.; Hawes, S. K. Semianalytic moderate-resolution
708 imaging spectrometer algorithms for chlorophyll a and absorption with bio-optical

709 domains based on nitrate-depletion temperatures. *J. Geophys. Res.*, **1999**, *104* (C3),
710 5403-5421; DOI: 10.1029/1998JC900082

711 67 Werdell, P. J.; Proctor, C. W.; Boss, E.; Leeuw, T.; Ouhssain, M. Underway sampling of
712 the marine inherent optical properties on the Tara Oceans expedition as a novel resource
713 for the ocean color satellite data production validation. *Methods in Oceanography*, **2013**,
714 7, 40-51.

715 68 Huot, Y.; Brown, C. A.; Cullen, J. J. Retrieval of phytoplankton biomass from
716 simultaneous inversion of reflectance, the diffuse attenuation coefficient, and sun-
717 induced fluorescence in coastal waters. *J. Geophys. Res.*, **2007**, *112*, C06013;
718 DOI:10.1029/2006JC003794

719 69 Falkowski, P. G.; Kolber, Z. Variations in Chlorophyll Fluorescence Yields in
720 Phytoplankton in the World Oceans. *Australian Journal of Plant Physiology*, **1995**, *22*,
721 341–355; DOI:10.1071/PP9950341

722 70 Merckelbach, L., Smeed, D., Griffiths, G. Vertical Water Velocities from Underwater
723 Gliders. *Journal of Atmospheric and Oceanic Technology*, **2010**, *27*(3), 547–563.
724 doi:10.1175/2009JTECHO710.1

725 71 Frajka-Williams, E.; Eriksen, C. C.; Rhines, P. B.; Harcourt, R. R. Determining Vertical
726 Water Velocities from Seaglider. *Journal of Atmospheric and Oceanic Technology*,
727 **2011**, *28* (12), 1641–1656; DOI:10.1175/2011JTECHO830.1

728 72, Lévy, M.; Klein, P.; Treguier, A. M. Impact of sub-mesoscale physics on production and
729 subduction of phytoplankton in an oligotrophic regime. *Journal of Marine Research*,
730 **2001**, *59* (4), 535-565.

731 73 Lévy, M. The modulation of biological production by oceanic mesoscale
732 turbulence. *Transport and Mixing in Geophysical Flows*. Springer: Berlin Heidelberg,
733 Germany, **2008**. 219-261. doi:10.1007/978-3-540-75215-8

734 74 Omand, M. M; D'Asaro, E. A.; Lee, C. M.; Perry, M. J.; Briggs, N.; Cetinić, I.;
735 Mahadevan, A. Eddy-driven subduction exports particulate organic carbon from the
736 spring bloom. *Science*, **2015**, *348*, 222-225, DOI: 10.1126/science.1260062.

737 75 Pietri, A.; Testos, P.; Echevin, V.; Chaigneau, A.; Mortier, L.; Eldin, G.; Grados, C.
738 Finescale vertical structure of the upwelling system off southern Peru as observed from
739 glider data. *Journal of Physical Oceanography*, **2013**, *43*, 631-646; DOI: 10.1175/JPO-
740 D-12-035.1

741 76 Webber, B. G. M.; Matthews, A. J.; Heywood, K. J.; Kaiser, J.; Schmidtko, S. Seaglider
742 observations of equatorial Indian Ocean Rossby waves associated with the Madden-
743 Julian Oscillation. *J. Geophys. Res. Oceans*, **2014**, *119*, 3714-3731;
744 DOI:10.1002/2013JC009657

745 77 Smyth, T.J. Penetration of UV irradiance into the global ocean. *Journal of Geophysical*
746 *Research*, **2011**, *116*, C11020. doi:10.1029/2011JC007183.

747 78 Platt, T.; Gallegos, C. L.; Harrison, W. G. Photoinhibition of photosynthesis in natural
748 assemblages of marine phytoplankton. *Journal of Marine Research*, **1980**, *38*, 687-701.

749

750

751

753 **Tables**

754 Table 1

Reference	Sampling Period	Position	Integration depth (m)	N	Mean (\pmStandard deviation) (g C m⁻² d⁻¹)
This Study	June 2013	48°N 16°W	Euphotic Zone	6	1.16 (0.5)
Chipman et al., (1993) ⁵⁶	May 1989	47°N 20°W	Euphotic Zone	11	0.84 (0.19)
Marra et al., (1995) ⁵⁷	June 1991	59.5°N 21°W	Euphotic Zone	4	1 (0.46)
Savidge et al., (1995) ⁵⁸	May/June 1990	47-60°N 20°W	Euphotic Zone	25	0.70 (0.32)
Bury et al., (2001) ⁵⁹	May 1990	47°N 20°W	Euphotic Zone	8	0.84 (0.50)
Painter et al., (2010) ²⁵	July 2006	49°N 16°W	Euphotic Zone	3	0.55 (0.22)

755

756 Table 1: Mean productivity rates from the NE Atlantic as reported in the literature. All

757 estimates were made using the ¹³C stable isotope method.

758

759

760

761

762 **Figures**

763

764 Figure 1: Modis aqua chlorophyll map showing location of study site and track of glider (black line)
765 and CTD position (blue dots). The black box in (a) indicates the location of the expanded map (b).

766

767 Figure 2: The scale factors calculated by optimisation of modelled attenuation of irradiance
768 against measured attenuation of irradiance (black X) with the 10 day moving window (black
769 line) and the standard deviation for each moving window (grey dashed line). The tick marks
770 on the x-axis represent the beginning of each month.

771

772 Figure 3: Time series of PAR corrected chlorophyll profiles, solid white line shows the mixed
773 layer depth (m) and the dashed white line shows the euphotic depth (m), calculated from the
774 glider PAR profiles.

775

776 Figure 4: Glider profiles of chlorophyll, uncorrected and PAR-corrected, compared to ship
777 based bottle samples of chlorophyll from acetone extracts. Mean profiles are shown as solid
778 lines. For cruises a. JC85, b. JC87 and c. JC90

779

780 Figure 5:

781 a) Daily mean PP from Seaglider dives compared with in situ ^{13}C estimates of
782 production. Error bars are the standard deviation of the PP calculated from all the
783 dives in one day. Water samples for the incubations were taken at dawn, a 12 hour
784 day for production is assumed.

785 b) Differences between integrated PAR-corrected glider primary production and the
786 uncorrected glider primary production compared with ^{13}C primary production
787 measurements.

788 c) Primary production estimates for the duration of glider deployments for SG566 and
789 NEODAAS 1 km daily product.

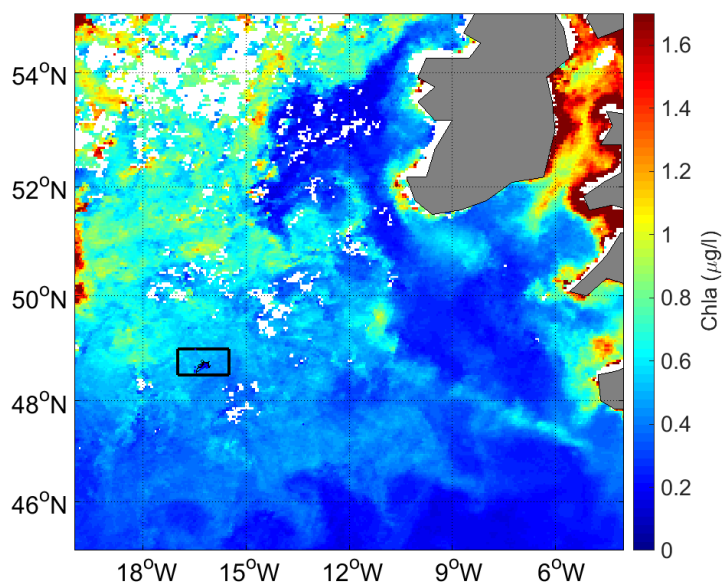
790

791 Figure 6: time series of PAR-corrected primary production profiles for SG566 for the entire
792 deployment, the solid white line is the mixed layer depth (m) and dashed white line as the
793 euphotic depth (1% of surface irradiance levels).

794

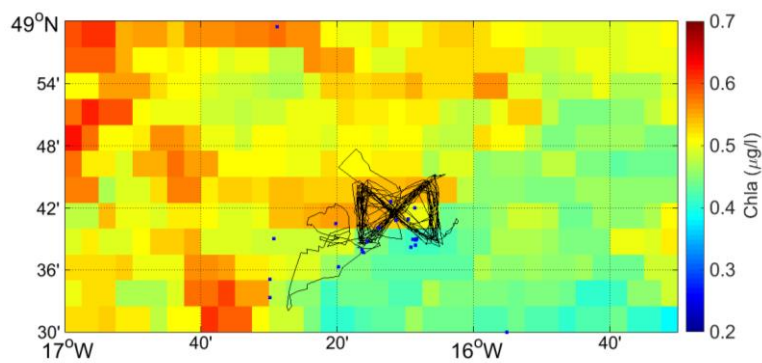
795 Figure 1

796 (a)



797

798 (b)



799

800 Figure 1: Modis aqua chlorophyll map showing location of study site and track of glider (black line)

801 and CTD position (blue dots). The black box in (a) indicates the location of the expanded map (b).

802

803

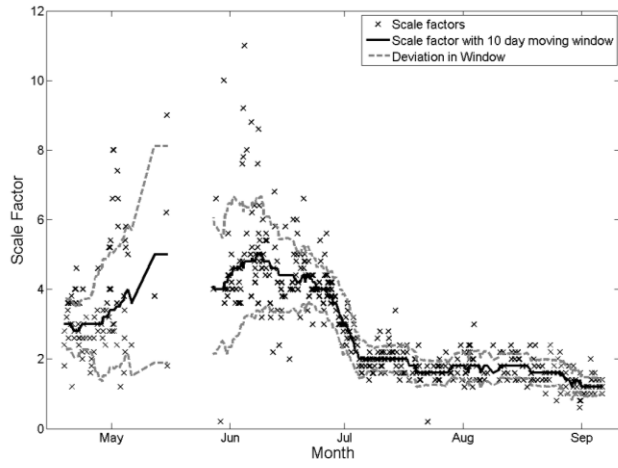
804

805

806

807

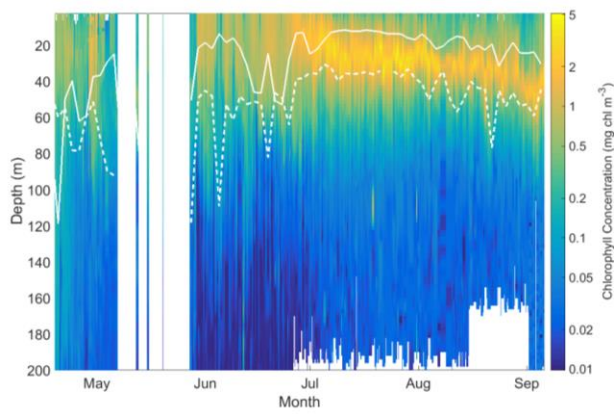
808 Figure 2



809

810

811 Figure 3



812

813

814

815

816

817

818

819

820

821

822

823

824

825

826

827

828

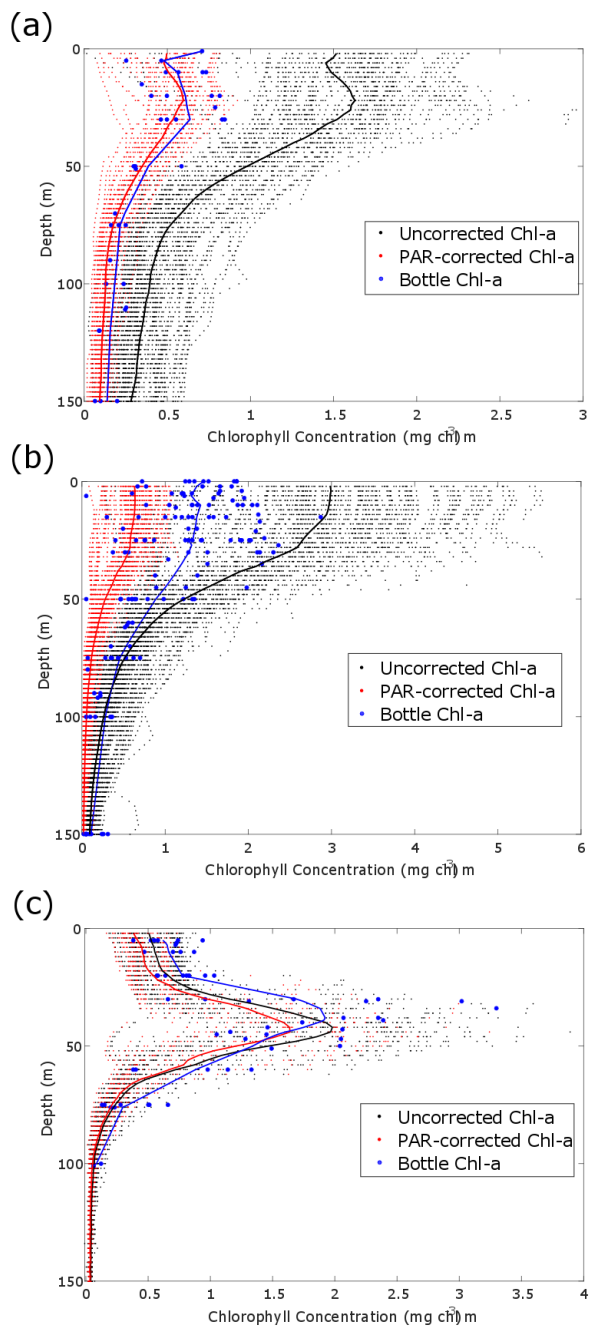
829

830

831

832

833 Figure 4



834

835

836

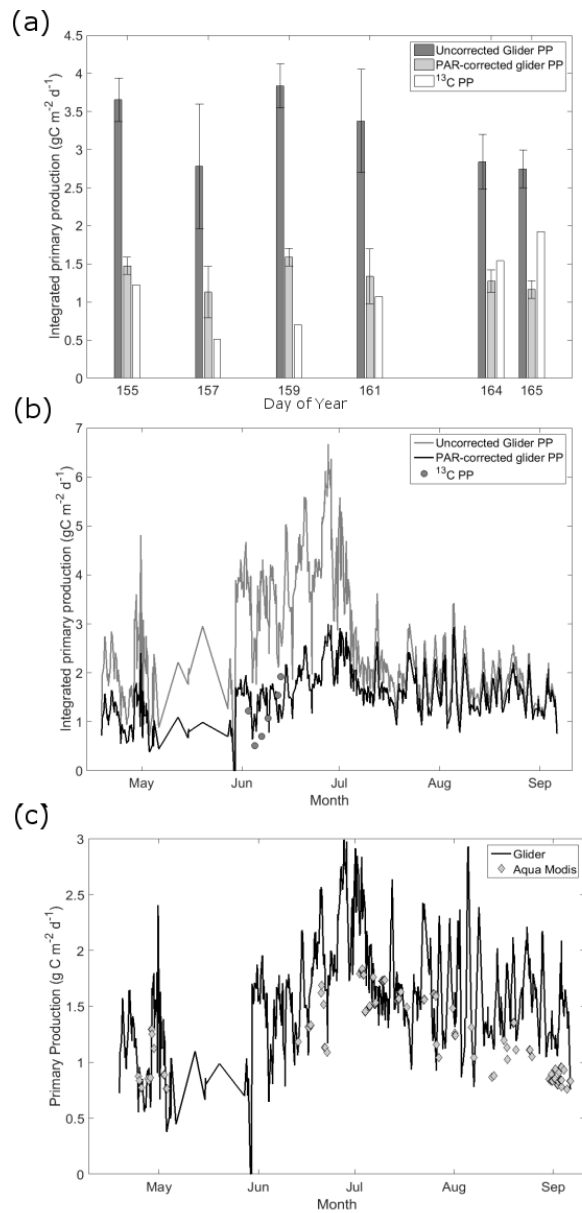
837

838

839

840

841 Figure 5

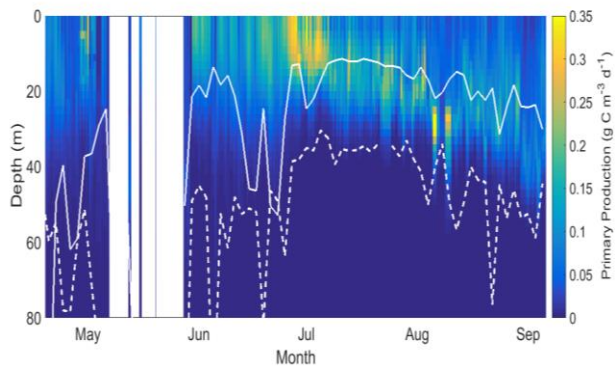


842

843

844

845 Figure 6



846

847